http://www.diva-portal.org

Postprint

This is the accepted version of a paper published in *Biochemistry*. This paper has been peer-reviewed but does not include the final publisher proof-corrections or journal pagination.

Citation for the original published paper (version of record):

Lundberg, M., Siegbahn, P E., Morokuma, K. (2008)
The mechanism for isopenicillin N synthase from density-functional modeling highlights the similarities with other enzymes in the 2-his-1-carboxylate family.
Biochemistry, 47(3): 1031-1042
http://dx.doi.org/10.1021/bi701577q

Access to the published version may require subscription.

N.B. When citing this work, cite the original published paper.

Permanent link to this version:
http://urn.kb.se/resolve?urn=urn:nbn:se:uu:diva-145473

Mechanism for Isopenicillin N Synthase from Density-functional Modeling Highlights the Similarities with Other Enzymes in the 2-His-1-carboxylate Family[†]

Marcus Lundberg[‡], Per E. M. Siegbahn[§] and Keiji Morokuma[‡*]

Fukui Institute for Fundamental Chemistry, Kyoto University, 34-4 Takano Nishihiraki-cho, Sakyo, Kyoto 606-8103, Japan

Department of Physics, Quantum Chemistry Group, Stockholm University, SE-106 91 Stockholm, Sweden

Running title: DFT mechanism for IPNS

[†] One of the authors (ML) acknowledges a Fukui Institute for Fundamental Chemistry Fellowship. The present work was in part supported by a CREST (Core Research for Evolutional Science and Technology) grant in the Area of High Performance Computing for Multi-scale and Multi-physics Phenomena from the Japan Science and Technology Agency (JST).

[‡] Kyoto University

[§] Stockholm University

[*] Corresponding Author: E-mail: morokuma@fukui.kyoto-u.ac.jp, Telephone:+81-75-711-7843. Fax: +81-75-781-4757.

Abbreviations: ACCO, 1-aminocyclopropane-1-carboxylic acid oxidase; ACmC, δ-(L-α-aminoadipoyl)-L-cysteinyl-L-S-methyl-cysteine; ACV, δ-(L-α-aminoadipoyl)-L-cysteinyl-D-valine; B3LYP, Becke's three parameter exchange-correlation functional; DFT, Density-functional theory; EXAFS: Extended X-ray absorption fine structure; IEFPCM, Integral equation formalism for the polarizable continuum model; INT, Intermediate; IPN, Isopenicillin N; IPNS, Isopenicillin N synthase; ONIOM, Our own N-layered integrated molecular orbital + molecular mechanics; QM:MM, Quantum mechanics:molecular mechanics; TST, Transition-state theory; TS, Transition state; 4-HPPD, 4-hydroxyphenylpyruvate dioxygenase;

Abstract. Isopenicillin N synthase (IPNS) catalyzes a key step in biosynthesis of the important β-lactam antibiotics penicillins and cephalosporins. Density-functional calculations with the B3LYP functional are used to propose a detailed mechanism for this reaction. The results support the general scheme outlined from experimental observations, with formation of a four-membered β-lactam ring followed by formation of a five-membered thiazolidine ring. However, an alternative mechanism for the heterolytic O–O bond cleavage is proposed that involves protonation of the distal oxygen by an iron-bound water ligand. This mechanism highlights the strong similarities that exist between IPNS and other enzymes of the 2-histidine-1-carboxylate family, especially pterin-dependent amino acid hydroxylases and α-keto-acid-dependent dioxygenases. Both activation of the cysteine β-C–H bond by an iron-bound superoxo radical and activation of the valine β-C–H bond by a ferryl-oxo species show reaction barriers close to the experimentally measured one. These results are in agreement with kinetic isotope experiments that suggest both C–H activation steps to be partially rate limiting. The ring-formation sequence is determined by the relative strengths of the two C–H bonds. Only the ferryl-oxo intermediate is capable of activating the stronger valine β-C–H bond.

Keywords. Non-heme, β-lactam, O–O bond activation, ferryl-oxo intermediate.

Isopenicillin N synthase (IPNS) catalyzes the formation of isopenicillin N, a key step in the synthesis of the important β-lactam antibiotics penicillins and cephalosporins (i-iv). Because an efficient fully synthetic route to isopenicillin N is still missing, the biosynthesis reaction is used in large-scale production. The enzyme is a potential target in the design of novel antibiotic compounds (v). Theoretical modeling helps to understand the requirements for successful biosynthesis, and can be a guide for substrate modification and/or protein engineering.

IPNS belongs to a family of oxygen-activated mononuclear non-heme iron enzymes with the 2-histidine-1-carboxylate binding motif. Other enzymes in the same family are: pterin-dependent hydroxylases, α-keto-acid-dependent dioxygenases, Rieske dioxygenases and extradiol dioxygenases (vi,vii). IPNS uses the four-electron oxidative power of O_2 to catalyze the transformation of the linear tripeptide substrate δ-(L-α-aminoadipoyl)-L-cysteinyl-D-valine (ACV) to isopenicillin N (IPN) (see Scheme 1). IPN is bicyclic with a four-membered β-lactam ring and a five-membered thiazolidine ring.

Compared to other reactions in the same enzymatic family, the substrate reaction in IPNS has a few unique features. IPNS is, together with 1-aminocyclopropane-1-carboxylic acid oxidase (ACCO), the only enzyme in this family where all four electrons required to reduce dioxygen come from the substrate (viii). In addition, no oxygen atom is incorporated into the substrate. Instead, abstraction of four substrate hydrogens, highlighted in Scheme 1, leads to the formation of two water molecules.

A proposal for the enzymatic mechanism of IPNS (iv) has been formulated based on incubation (ii), spectroscopic (ix-xi) and crystallographic studies of substrate and substrate analogs (iv,xii-xvii) (see Scheme 2). Binding of the ACV substrate results in a five-coordinate iron site where iron is ligated by His214, Asp216, His270 (*Aspergillus nidulans* numbering), the

substrate thiolate, and one water molecule (iv). Although there are many highly conserved residues in IPNS, the three iron ligands are so far the only ones that seem to be critical for activity (the D216E mutation retains 1 % activity) (xviii-xx). Iron is in the high-spin Fe(II) state (S=2) (ix). This is the preferred spin state for this family of enzymes and reflects the weak ligand field of the coordinating amino acids (xxi).

Substrate binding increases the enzyme's affinity for oxygen, either by increasing the hydrophobicity of the active site (xvi) and/or by tuning the Fe(II)/Fe(III) redox potential. No O_2-bound state has yet been experimentally observed, instead an NO-bound analogue serves as a model compound (xi,xii,xxii). NO binds in a position trans to Asp216, and it is assumed that O_2 binds in the same position (see Scheme 2).

Kinetic isotope effects (xxiii) and the crystallographic observation of a monocyclic β-lactam ring in the substrate analogue ACmC (xiii) suggest that formation of the four-membered β-lactam ring is completed before formation of the C–S bond in the five-membered thiazolidine ring. The iron-bound dioxygen species should therefore first activate the cysteine β-C–H bond, leading to a ferrous peroxide (Fe(II)–OOH). According to the proposal in reference iv, the peroxide should then abstract the valine N–H proton to generate a ferryl-oxo (Fe(IV)=O) species and a water molecule. Concerted with ferryl-oxo formation, the valine nitrogen performs a nucleophilic attack on the cysteine β-carbon, which leads to cyclization of the β-lactam ring.

Generation of a high-valent ferryl-oxo species is a common theme, shared by many non-heme iron enzymes. This intermediate is often formed by oxidation of a cofactor like α-keto-acid or tetrahydrobiopterin (vi) but in IPNS it is generated by the two-electron oxidative cyclization of the substrate. There is little doubt that a ferryl-oxo intermediate is formed in IPNS, but a previous study using density-functional theory (DFT) disfavored parts of the mechanism

proposed in reference iv, because the barrier for O–O bond cleavage was prohibitively high (xxiv). An alternative mechanism was suggested instead, but a re-examination of the results from reference xxiv raised some questions regarding this alternative proposal.

After β-lactam ring formation, the enzymatic mechanism seems straightforward. The high-valent ferryl-oxo species is a powerful oxidant and can be used in a variety of reactions, e.g. oxygenations, hydroperoxidations and epoxidations. In IPNS it should activate the C–H bond of the tertiary valine β-carbon. This creates a carbon-centered substrate radical and a ferric-hydroxy (Fe(III)–OH) species. Independent deuterium kinetic isotope effects for both the cysteine β-carbon and for the valine β-carbon suggest that both C–H activation steps are at least partially rate-limiting (xxv).

The aliphatic carbon radical then attacks the cysteine thiolate to close the thiazolidine ring and complete the formation of isopenicillin N (see Scheme 2). An alternative reaction, observed in many other enzymes that form ferryl-oxo intermediates, is hydroxylation of the substrate in an oxygen rebound mechanism (vi). The reason why IPNS preferentially catalyzes ring formation rather than hydroxylation still remains to be explained, and will be addressed in the present study.

The present re-investigation of the catalytic mechanism in IPNS using density functional modeling was prompted by the new information available from experimental (vii) and theoretical (xxvi,xxvii) studies recently performed on other members of the 2-histidine-1-carboxylate enzyme family. The purpose of the present study is to find a mechanism for O–O bond heterolysis, consistent with the experimentally estimated reaction barrier of 16.8 kcal/mol (xxviii). The expected accuracy of density functional calculations for transition metal enzymes is in the 5 kcal/mol range. This level of accuracy makes it difficult to calculate and compare exact

rates of individual steps, but the method is in general accurate enough to discriminate between different mechanistic proposals for the same reaction.

COMPUTATIONAL METHODS

All calculations were performed on an active-site model of the iron center. The model includes Fe, the side chains of the amino acids coordinating iron (His214, Asp216, and His270), the water ligand (WAT398) (iv), and the cysteine-valine part of the substrate where the chemical transformation occurs (see Figure 1). Only the first-shell amino acids have been included, partly because they are the only ones known to be essential for catalysis (xviii). Histidine is modeled as 4-methylimidazole, and aspartate is modeled as acetate. The initial model system (Model A) consists of 65 atoms.

Initial coordinates are taken from the X-ray structure 1BLZ (1.45 Å resolution), which represents the ACV-Fe(II)-NO state, and NO is replaced by O_2. To avoid artificial changes in geometry caused by an incomplete hydrogen-bond network in the truncated model, Cartesian coordinates of selected atoms were kept frozen during optimizations (see Figure 1). However, during the reaction, the substrate goes from a linear molecule to a bicyclic one, and the coordinates of the substrate can therefore not be kept frozen in the same position during the entire reaction. To minimize problems with artificial hydrogen bonds, two changes are made to the model during the reaction. Starting from the full model described above (Model A), Model B excludes the carboxylate group before the closing of the β-lactam ring, while Model C also excludes the water molecule formed after O–O bond heterolysis (see Figure 1). Model A has a net charge of -1 while models B and C are neutral.

Calculations are performed using Gaussian03 (xxix). Geometries are optimized using the hybrid functional B3LYP (xxx) and the 6-31G(d) basis set. Final energies are evaluated using the 6-311+G(d,p) basis set. Hybrid density functional is the only method that can treat systems of the present size with reasonable accuracy. The popular B3LYP functional has been shown to perform relatively well for a large number of different transition-metal applications (xxxi), but errors in the 5 kcal/mol range have to be expected.

All calculations are performed using the unrestricted formalism. Selected stationary points have been calculated with different spin multiplicities (septet, quintet, and triplet). Based on previous results from enzymes with similar active sites, the singlet state is assumed to be unstable (xxvi). For the reactant (Fe–O_2 side-on), the singlet state is unstable by approximately 20 kcal/mol. Open-shell species with antiferromagnetic coupling have not been corrected for spin contamination. For the quintet Fe–O_2 species (end-on binding), the correction using the Heisenberg Hamiltonian formalism (xxxii) would have been 0.7 kcal/mol and for the quintet intermediate **16** (Fe(III)–OH with a substrate radical) it would have been <0.2 kcal/mol. For intermediate **16**, calculations on alternative spin states have been performed with a model without methyl groups on the amino-acid models.

Electronic energies are corrected by adding zero-point, thermal and solvent contributions. These effects are evaluated using the same basis set as in the optimization (6-31G(d)). Zero-point energy and thermal corrections are taken from un-scaled frequencies of a fully optimized model without methyl groups on the amino-acid models. Zero-point corrections are important for the C-H bond activation steps because they lower the barriers of these steps by 3–5 kcal/mol. Solvent corrections are calculated using IEFPCM (xxxiii) with a dielectric constant of 4, mimicking the interior of a protein. In the present calculations, the solvent effects are particularly large for

intermediate **5** (+7 kcal/mol). This large effect indicates a slightly unbalanced computational model. The main problem is the substrate carboxylate that has no hydrogen-bonding interactions in the reactant, but is involved in hydrogen binding with a peroxide species in intermediate **5**. Fortunately, the calculated rate-limiting barriers do not depend on the energy of this intermediate.

All reported energies represent an estimate of ΔG or $\Delta G^{\ddagger}$ for each stationary point. Comparisons with the experimentally determined rate are made by using the standard form of transition-state theory (TST). In TST a rate of 3.2 s^{-1} corresponds to a barrier of 16.8 kcal/mol (xxviii).

RESULTS AND DISCUSSIONS

The modeled mechanism for formation of isopenicillin N involves a large number of stationary points. To facilitate the discussion, stationary points are assigned numbers (appearing in bold face) based on the order they appear along the reaction coordinate. When necessary, the nature of the stationary point is indicated by a label, TS for transition state and INT for a reaction intermediate. For some steps, e.g. bond rotations, transition states have not been optimized and two intermediates may therefore follow directly after each other in the potential energy diagram. Structures that are stationary states on the B3LYP/6-31G(d) surface used for optimization, but not after the energy has been corrected for basis set, zero-point, thermal, and solvent effects are labeled "TS" and "INT", respectively. For the most stationary points, only the quintet state has been modeled. States with septet and triplet multiplicities are indicated by left superscript, e.g. ^{7}**1** and ^{3}**1**, respectively.

A. Cys-β-C-H activation.

The present investigation includes all the steps involved in the chemical transformation of the substrate, with the exception of substrate binding. An important potential consequence of substrate binding is deprotonation of the thiol group upon ligation to iron. It is difficult to calculate protonation states in proteins using active-site models, but for the substrate, the protonation state can be assigned from indirect observations. For the Fe(II)-ACV complex, EXAFS gives an Fe-S distance around 2.35 Å (x,xi) and this can only be reproduced with a deprotonated substrate (Fe-S distance of 2.32 Å). Models with protonated thiols give Fe–S distances >2.50 Å. The acceptor of the thiol proton is assumed to be outside the active-site model.

The O_2 molecule enters the active site after substrate binding. Using the present active-site model, O_2 binding was previously found to be endergonic by 10.6 kcal/mol (xxxiv). A high endergonicity for this step is in line with previous experience from active-site models (xxvi,xxxv,xxxvi), but seems to be in contradiction with the observed reactivity of these enzymes. ONIOM QM:MM calculations were therefore performed on the O_2 binding step in IPNS and the results confirm that binding of dioxygen is not accurately handled by active-site models. Including the protein environment stabilizes O_2 binding by 8–10 kcal/mol, and gives an almost thermoneutral reaction, as reported by us previously (xxxiv). In the present investigation, the dioxygen-bound state is therefore taken as the reference state.

Throughout the present study, assignments of electronic structures and oxidation states are made based on bond distances and Mulliken spin populations. In the reactant (^{7}**1** in Figure 2) iron has a spin population of 4.09. This corresponds to a high-spin ^{6}Fe(III) state, although ^{6}Fe(III) formally has five unpaired electrons in the 3d orbitals. Using essentially the same

methods as in the present study, spin populations of 3.7–3.8 approximately corresponds to ^{5}Fe(II), of 4.0–4.2 to ^{6}Fe(III), and of 3.0–3.3 to ^{5}Fe(IV) (xxxvii). The difference between the calculated spin populations and the formal number of unpaired d-electrons is due to backdonation from ligand β-orbitals. Consequently, spin formally assigned to d-orbitals on Fe is delocalized to all the ligands. However, the amount of delocalization is almost the same for all iron complexes of the same oxidation state, and spin populations are therefore good indicators of the oxidation states of high-spin iron systems. In the B3LYP description, the reactant (^{7}**1**) is thus a ferric-superoxo species (Fe(III)–OO^-) obtained by electron transfer from Fe(II) to an anti-bonding 3π orbital in O_2. This assignment is consistent with the detailed orbital analysis in reference xxii.

The most stable O_2-bound state is a septet with side-on coordination (both oxygen atoms coordinate to iron) (^{7}**1**) and this is taken as the reference (zero) of energy. The relative energy of the most stable quintet state (^{5}**2** with end-on coordination having one coordinating oxygen) is +2.9 kcal/mol (see Figure 3). With the present accuracy, this energy difference is too small to allow a definite assignment of the spin state in the enzyme. Both these states are assigned as ferric-superoxo states and the major difference is the alignment of the spin on the superoxo radical (parallel or antiparallel to the spins on iron). There exists also a triplet state (^{3}**2**) at +4.2 kcal/mol. This state has substantial Fe(II)–O_2 character with a slightly shorter O–O bond (see reference xxxiv for details).

Dioxygen binding to the high-spin iron center removes the constraints of a formally spin-forbidden reaction between triplet oxygen and the closed-shell ACV substrate. According to Scheme 2, the next step is activation of the Cys-β-C–H bond. Brown et al have recently shown

that the frontier molecular orbital of the Fe(III)-superoxide, the O_2 π^* orbital, is oriented so that it forms a σ overlap with the hydrogen (xxii).

Proceeding from the stable reactant (^{7}**1**) on the septet surface, a transition state (^{7}**3**) is reached at 20.6 kcal/mol. This leads to a high-spin ferric peroxide (Fe(III)–OOH) and a substrate radical centered on the β-carbon (^{7}**4** INT at 11.0 kcal/mol). To reach a septet state, the spin on the substrate radical is necessarily aligned in parallel with the spins of the five d-electrons in Fe(III).

Although the quintet state is not the stable reactant, the reaction on the quintet surface turns out to be more favorable because it leads to a more stable product. On the quintet surface, the barrier for Cys-β-C–H activation (^{5}**3** TS) is at 14.6 kcal/mol, significantly lower than on the septet surface. This step should be at least partially rate-limiting, and compared to the experimental barrier of 16.8 kcal/mol, the presently calculated barrier is slightly underestimated.

Because the reaction occurs on the quintet surface, a transition between the septet and the quintet surfaces must occur. The most stable conformation on the quintet surface is end-on binding of dioxygen (^{5}**2** INT) (see reference xxxiv for details). Previous calculations on similar active sites showed that the minimum-energy crossing point between septet and quintet was located <1 kcal/mol above the quintet structure (xxvi). Together with strong spin-orbit coupling in the transition-metal system, the spin transition should therefore be very fast and not affect the rate of the reaction.

The resulting quintet intermediate (^{5}**4** INT) is relatively stable (-4.6 kcal/mol, see Figure 3). A rotation of the FeO–OH bond results in an even lower energy (-10.8 kcal/mol) due to formation of better hydrogen bonds with the carboxylate group of the substrate (^{5}**5** INT shown in Figure 4). In the real protein, the carboxylate is included in a hydrogen-bonding network with the

residues Tyr189, Arg279 (through a water molecule) and Ser281. When these additional residues are included in the QM model, the hydrogen bond between substrate and peroxide does not develop. In the new model the relative energy of intermediate ^{5}**5** INT increases by approximately 3 kcal/mol. Fortunately, the barrier for the following transition state (^{5}**6** TS) changes by less than 1 kcal/mol. Since these corrections do not affect the conclusions of the present paper, they have not been included in the results.

Looking closer at the electronic structure of the intermediate ^{5}**4**, it is clear that it corresponds to a ferrous peroxide (Fe(II)–OOH) and a double bond between carbon and sulfur. This assignment can be derived from the low spin density on the cysteine β-carbon (-0.07), the spin population on iron (3.81), the shorter C–S distance (1.64 Å compared to 1.85 Å in the reactant), and the longer S–Fe distance (2.65 Å compared to 2.32 Å in the reactant), see Figure 4 for details.

The very large difference in stability between the septet (^{7}**4**) and the quintet (^{5}**4**) intermediates can be explained by an additional electron transfer from the substrate to iron. This electron transfer can only take place in the quintet state, because the unpaired substrate electron must be transferred to an empty β-orbital on Fe(III). Activation of the Cys-β-C–H bond thus leads to abstraction of one proton and two electrons from the substrate. This may not seem consistent with the reaction described by transition state ^{5}**3**, since it has all the characteristics of a hydrogen atom transfer, with significant spin (0.39) developing on the carbon atom (see Figure 2). Following the intrinsic reaction coordinate (IRC) from ^{5}**3** TS increases the spin on carbon further to a maximum of 0.65, but this substrate radical is not an intermediate in the present calculations. Instead, the second electron is transferred from the substrate and the system relaxes to the Fe(II)-OOH intermediate without any barrier.

The corresponding intermediate on the triplet surface ^{3}**4** also represents an Fe(II)–OOH state, but it is significantly higher in energy (by 13 kcal/mol) than the quintet state, since it requires intermediate spin on iron Fe(II).

There appears to be a relatively straightforward reason why Cys-β-C-H activation, and therefore β-lactam ring formation, occurs prior to Val-β-C–H activation. Looking at the substrate model only, the strength of the Cys-β-C–H bond is significantly lower (by 11 kcal/mol) than that of the Val-β-C–H bond. Carbon-centered radicals are stabilized in dialkyl sulfides (xxxviii) and the presence of the thiolate should therefore make the C-H bond weaker. The transfer of the second substrate electron to iron also helps to stabilize the transition state ^{5}**3**. The Cys-β-C–H bond can therefore be activated by the comparably weaker oxidant Fe(III)–OO^{-}, while the corresponding bond of the valine β-carbon can only be activated by the strong Fe(IV)=O oxidant, formed after O–O bond heterolysis.

The description of the C–H activation step in the present study is different from that of the previous DFT study by Wirstam *et al* (xxiv). In that study, the presently proposed mechanism was not supported because the barrier for C–H activation was only 1.1 kcal/mol, which is not consistent with kinetic isotope experiments showing that this step is partially rate limiting (xxiii). A possible explanation of the results in reference xxiv is that the low barrier is caused by an unstable electronic configuration in the reactant. The present reactant ^{7}**1** is an Fe(III)–OO^{-} state, similar to the ones obtained for other oxygen-activated non-heme enzymes (xxvi), while the reactant in reference xxiv is an Fe(II)-state with significant spin on the substrate thiolate but very low spin density on oxygen. In the present investigation, that state could not be reproduced, even when the same model was used. However, if the transition state and resulting intermediate represent the same states in the two studies (they have similar spin populations), the present

Fe(III)–OO$^-$ reactant (^{7}**1**) is approximately 10 kcal/mol more stable than the reactant used in reference xxiv.

The study by Wirstam *et al*. instead preferred a reaction where Fe–O_2 accepts a proton from an external donor before the C–H bond is activated. This leads to an acceptable barrier for O–O bond cleavage in a reaction with Cys-β-C–H. However, in the present study the O_2 species has a lower proton affinity than the substrate thiolate (by 15 kcal/mol in ^{7}**1**). Since EXAFS data suggest that there is no proton on the thiolate, see discussion above, dioxygen should therefore not be protonated either. If the minimum energy penalty for protonating O_2 is 15 kcal/mol, the transition state for O–O bond cleavage in reference xxiv becomes too high (30 kcal/mol).

B. O–O bond cleavage and β-lactam ring formation.

After generation of the peroxide intermediate, a seemingly attractive mechanism is abstraction of the valine N–H proton by the peroxide to generate a ferryl-oxo (Fe(IV)=O) species and a water molecule. At the same time, the valine nitrogen should perform a nucleophilic attack on the cysteine β-carbon, which leads to formation of the β-lactam ring (see Scheme 2). However, as mentioned in the Introduction, one of the main conclusions from the previous DFT study of isopenicillin N synthase was that this mechanism had an exceedingly high barrier (xxiv). The present study supports that observation. Cleaving the O–O bond by protonation from the valine N–H group has a barrier of 30.9 kcal/mol and occurs after the C–N bond in the β-lactam ring is almost formed (C–N distance of 1.62 Å). Although the two models are slightly different, this transition state is very similar to the one optimized in reference xxiv. With the present model, all other tested combinations of concerted and step-wise reactions involving these three bonds gave similar or higher barriers.

In search for an alternative mechanism, it was noted that formation of a ferryl-oxo intermediate is a common step for many mononuclear non-heme enzymes. A number of these reactions have also been modeled theoretically, see e.g. reference xxvii, and ideas for alternative mechanisms were therefore sought among this enzyme family. In several enzymes, formation of Fe(IV)=O from an Fe(II)–OOR species generates a negative charge on one of the other iron ligands. In α-keto-acid-dependent dioxygenases a carbonyl becomes the anionic part of a carboxylic acid, while in pterin-dependent hydroxylases O–O bond cleavage leads to formation of an HO–Fe(IV)=O species (xxvi). More specifically, in pterin-dependent hydroxylases, O–O bond heterolysis is assisted by a ligating water molecule that donates a proton to the distal oxygen and thereby generates the HO-Fe(IV)=O intermediate.

IPNS also has a water ligand bound to iron and abstracting a proton from this water leads to O–O bond cleavage with a barrier of 9.8 kcal/mol. The calculated potential energy diagram for the full isopenicillin N reaction, including O–O bond cleavage, is shown in Figure 5. The initial reaction coordinate, starting from the Fe(II)–OOH intermediate ^{5}**5,** describes homolytic O–O bond cleavage with a single electron transfer from iron to an anti-bonding O–O σ* orbital. The transition state (^{5}**6** TS in Figure 4) involves only O–O bond breaking (bond distance of 1.84 Å) and leads to a shallow minima (^{5}**7** INT) which is essentially Fe(III) (Mulliken spin of 4.10) antiferromagnetically coupled to a hydroxyl radical (Mulliken spin of -0.65). From this metastable intermediate, a proton is transferred from the iron-bound water ligand, coupled to a second electron transfer from iron, via ^{5}**8** TS (in Figure 4). The total O–O bond cleavage reaction is therefore heterolytic and leads to formation of a water molecule and an HO–Fe(IV)=O intermediate (^{5}**9**). The reaction is highly exothermic (see Figure 5).

The pathway for O–O bond cleavage looks highly similar to modeled reactions for pterin-dependent hydroxylases (xxxv), a biomimetic non-heme iron complex (xxxix), and the α-keto-acid-dependent clavaminate synthase (xl) (see Scheme 3). All of them show an initial O–O bond elongation, coupled to a single-electron transfer, followed by a second electron transfer leading to the Fe(IV)=O species. For all modeled reactions, the O–O bond distances for the intermediate as well as for the first transition state are very similar, while the O–O bond distance for the second transition state seems to depend on the exothermicity of the reaction (shorter bond length for more exothermal reactions). Whether or not the intermediate appears on the calculated potential energy surface seems to be determined by minor details, i.e. the modeled reaction is step-wise for clavaminate synthase but not in 4-HPPD (xli), despite both of them performing the same reaction, oxidative decarboxylation of the α-keto-acid cofactor. For all practical purposes, O–O bond heterolysis can be considered as a concerted reaction.

Another common feature for the three enzymes shown in Scheme 3 is that O–O bond cleavage is not the rate-limiting step. Instead the barrier for two-electron oxidation of the co-factor (or substrate in the case of IPNS) is consistently higher.

Despite the overall similarities, there are also differences among the three reactions in Scheme 3. Most noticeably, in the pterin-dependent hydroxylases and clavaminate synthase the O_2 group initially binds in a position trans to a histidine ligand while in IPNS it binds trans to the carboxylate. Another difference is that the clavaminate synthase active site is modeled as five-coordinate after release of CO_2 in the preceding reaction, while the other models are six-coordinate. The barrier for O–O bond cleavage is higher in IPNS than in the pterin-dependent hydroxylase and clavaminate synthase (9.8 kcal/mol compared to 4.8 and 4.7 kcal/mol respectively).

The high barrier for O–O bond cleavage by protonation from the valine N–H (the mechanism proposed in reference iv) is slightly puzzling. After accepting two electrons from the substrate but only one proton, the Fe–OOH species has a high proton affinity and it is not clear why Val-N–H is not a suitable proton donor. Closing the β-lactam ring breaks the C=S double bond and regenerates the negative thiolate iron ligand. This reaction thus also creates a new negative iron ligand. Despite this, the presently modeled barrier is very high. Although a number of different reaction pathways have been explored, this pathway should not be completely ruled out until a convincing explanation for the high barrier can be found. A possible explanation would be that as long as the C–N bond of the β-lactam ring has not yet formed, Val-N–H is a worse proton donor than water bound to iron. Protonation from Val-N-H in intermediate ^{5}**7** therefore requires simultaneous O–O bond cleavage and C–N bond formation. However, these reactions are not strongly coupled in the present calculations, and the barriers for the two separate reactions seem to be added.

In the Fe(IV)=O intermediate (^{5}**9** INT in Figure 6) the spin on iron is 3.21 while substantial spin is located on the oxo group (Mulliken spin of 0.46). The Fe–O bond formally has double-bond character that originates from the distribution of eight electrons in five FeO orbitals (σ, π, π*). Since the two π* orbitals are singly occupied, this causes significant spin to be assigned to oxygen. The identity of the Fe(IV)-oxo state is supported by the calculated Fe–O distance of 1.64 Å, which is similar to experimentally measured distances for Fe(IV)=O complexes (1.62 Å) (xlii,xliii). Experiments suggest that the high-spin complex is the most stable (xliv) and computationally, triplet (^{3}**9**) and septet (^{7}**9**) states are unstable by 5.2 and 10.3 kcal/mol respectively. Because these states are unstable also in the Fe(II)–OOH state (^{5}**4** INT), O–O bond cleavage was not modeled for these spin states.

An alternative reaction pathway for O–O bond cleavage on the quintet potential energy surface can be explored by decreasing the O–O bond distance from the Fe(IV)=O intermediate (^{5}**9**). At an O–O distance of 2.0 Å, the energy is lower than for the reaction path outlined above, but the electronic configuration still represents an Fe(IV)=O state and the proton resides on the water molecule. Decreasing the O–O bond distance further increases the energy for this configuration and no low-lying transition state could be found.

The presently modeled O–O bond heterolysis reaction occurs without direct involvement of the substrate in the bond cleavage step. However, the substrate has already played a critical role because it contributed the two electrons required for formation of the Fe(IV)=O intermediate already in the first reaction step (^{7}**1**→^{5}**4**). The ACV substrate has at this stage thus already performed the same role as the α-keto-acid and tetrahydrobiopterin cofactors perform in other non-heme enzymes.

To finally close the β-lactam ring, the substrate should lose the valine N–H proton and form a bond between the cysteine β-carbon and the valine nitrogen. Formation of the C–N bond recreates the negative thiolate ligand, a process that is likely to increase the proton affinity of the water-derived iron ligand and lead to its protonation. From a modeling perspective, this is a complicated reaction that requires an accurate description of the correct acceptor of the N–H proton, the proton-transfer pathway to the hydroxo ligand, and the changes in hydrogen bond patterns that occur during the reaction. The present model is too limited to take all these factors into account. However, to illustrate that the barrier is not prohibitively high, a mechanism for ring closure has still been calculated. Neither the barrier nor the exact reaction mechanism should probably be taken literary and, due to the tentative nature of this mechanism, it will be only briefly described.

The assumption that the Fe–OH ligand directly accepts the Val-N-H proton is reasonable and enables a potential energy profile to be constructed without use of any external parameters, i.e. proton affinities of the surrounding media. In the modeling, the newly formed water molecule act as a proton shuttle between the substrate and the hydroxo group. The substrate carboxylate is removed from the model to avoid the formation of artificial hydrogen bonds (Model B).

On the uncorrected surface, closing of the β-lactam ring proceeds through several stationary points but after all corrections have been added, only one transition state remains (^{5}**12** TS in Figure 6). The presence of a single transition state shows that ring closure is a concerted reaction with proton transfer from the valine N–H group to the Fe–OH ligand occurring simultaneously with C–N bond formation. Although the optimized transition structure (^{5}**12** TS) shows that proton transfer has been completed at an early stage of the reaction, this might be an artifact from the optimization on the uncorrected potential energy surface.

The calculated barrier for β-lactam formation through ^{5}**12** TS is relatively high, 18.4 kcal/mol. This barrier is close to the experimental limit of 16.8 kcal/mol and could represent another rate-limiting step of the IPNS reaction. The common interpretation is that IPNS has two rate-limiting steps, activation of the valine and the cysteine β-C–H bonds, but the proposed mechanism does not contradict the available experimental data.

First, the present accuracy only allows a determination of relative energies with an accuracy of 3-5 kcal/mol. In addition, the present mechanism is tentative and lower barriers could exist for other proton transfer pathways. The exact height of the barrier must therefore be treated with considerable caution. If the barrier is 3-5 kcal/mol lower (i.e. 13-15 kcal/mol), it will be kinetically silent compared to the C–H activation steps where the barriers experimentally are known to be around 17 kcal/mol.

Second, the suggestion of two rate-limiting steps is based on kinetic isotope experiments that show independent effects for both cysteine β-C–H and valine β-C–H protons (xxiii). Although these experiments clearly show that no other reaction step can have a higher barrier, the results do not exclude a third reaction step with a marginally lower barrier. Deuterium substitution increases the barriers of the C–H bond activation steps, and the kinetic effect of a potential third step would largely disappear.

A signature of a third rate-limiting step would be an isotope effect also for the valine-N–H proton. Unfortunately, the lack of an effect would not be conclusive. It could either mean that the barrier for β-lactam ring formation is lower than presently modeled, or that the ring closure transition state is dominated by formation of the C–N bond (as in ^{5}**12** TS).

In total, formation of the monocyclic β-lactam form of the substrate (^{5}**13** INT) from the open form (^{5}**9** INT) is slightly exothermic (see Figure 5). The open form should therefore not be observed in equilibrium conditions, but could possibly be detected as a metastable species. Crystallographic studies of the substrate analogue AcMC, that cannot undergo the second ring formation step, show that the closed β-lactam ring (xiii) is indeed the stable form.

Despite the Fe-center not being redox active during the reaction, β-lactam ring formation does probably not occur before generation of the Fe(IV)=O species (i.e. from intermediate ^{5}**5**). Ring closure regenerates the thiolate ligand since it breaks the C=S double bond (see Scheme 2), and this reaction is more favored when the oxidation state of iron is Fe(IV) compared to Fe(II). The detailed reaction mechanism cannot be calculated with the present model, because there is no suitable acceptor for the valine N–H proton (in intermediate ^{5}**5** the iron ligand is still water, not a hydroxo group). However, the energy required to shorten the C–N bond without proton transfer is significantly lower in ^{5}**9** INT (Fe(IV)) than in ^{5}**5** INT (Fe(II)).

C. Val-β-C–H activation and thiazolidine ring formation.

The final stage of the reaction is activation of the C–H bond of the valine isopropyl group by Fe(IV)-oxo, followed by formation of the second substrate ring. The modeled reaction supports the mechanistic proposal in Scheme 2. The reaction is complicated by the fact that in the X-ray structure, the Val-β-C–H bond actually points away from the iron center. A possibility is that the valine isopropyl group rotates during formation of the β-lactam ring, but in the present model, this did not occur (see ^{5}**13** INT in Figure 7). In an active-site model, the isopropyl group can be easily rotated so that the C–H bond faces the iron center (^{5}**14** INT). The Fe(IV)-oxo group then abstracts a hydrogen from the valine isopropyl group with a total barrier of 15.3 kcal/mol (see ^{5}**15** TS in Figures 5 and 7). In this step, the high-spin Fe(IV)=O complex is transformed into a high-spin Fe(III)–OH species, while the unpaired electron of the aliphatic radical has its spin aligned opposite to the spins on the ferric iron. The calculated barrier of 15.3 kcal/mol is rather close to 14.6 kcal/mol calculated for the other rate-limiting step, activation of the cysteine β-C–H bond (^{5}**3** TS).

The substrate radical is proposed to be a short-lived reaction intermediate (^{5}**16** INT in Figure 8). Compared to the most stable Fe(IV)=O state (^{5}**13** INT), the relative energy of this state is -1.8 kcal/mol (see Figure 5). The unpaired electron on carbon does not couple strongly with the electrons on iron so for this intermediate there exists a close-lying septet state (^{7}**16**). However, the septet state is unstable both in the forward and backward directions and should therefore not participate in the reaction.

In the final step, the carbon radical attacks the thiolate coordinating to iron and forms a new C–S bond, thus closing the thiazolidine ring and completing the formation of the bicyclic

isopenicillin N molecule. The barrier for this step is only 4.5 kcal/mol (see Figure 5). During the reaction an electron is transferred from the substrate to iron and, judging by the spin populations, this electron transfer occurs concerted with C-S bond formation. The spin population on carbon changes from -0.90 in the intermediate ^{5}**16** to -0.67 in the transition state ^{5}**17** (see Figure 8).

The final product is a bicyclic substrate with both β-lactam and thiazolidine rings, weakly coordinated to an Fe(II) complex. In the present active-site model, the IPN product loses coordination to iron (Fe-S distance of 4.2 Å), which is not supported by X-ray data (Fe–S distance of 2.87 Å) (xiii). With a relative weak coordination, the exaggerated mobility of the active-site model leads to formation of artificial hydrogen bonds that successfully compete with iron coordination. As a consequence, the exothermicity of the final step may therefore be slightly overestimated with the small basis set. Large basis, and solvent corrections may instead favor the tighter bound structure and for a given structure it is difficult to know which effect that will dominate. In any case, the relative energy of the product should be considered as approximate.

The results for thiazolidine ring formation are very similar to those obtained in the previous DFT study (reference xxiv). However, the increased model size, i.e. including the methyl groups close to the valine β-carbon, significantly stabilizes the carbon radical intermediate.

Finally, protonation of the Fe(II)–OH group should generate the second water molecule. Because no external proton donor is included, this reaction step has not been modeled. The donor should be the same, or similar, to the group that accepted the S–H substrate proton upon substrate binding. It is therefore noted that the proton affinity of the Fe(II)–OH group is similar to the proton affinity of the thiolate in the reactant complex. The protonation of the Fe–OH

ligand to complete the formation of two water molecules from dioxygen should therefore be relatively straightforward.

Finally, an attempt was made to understand why IPNS performs oxidative cyclization instead of substrate hydroxylation (i.e. prefers the rebound of sulfur over the rebound of oxygen). Starting from the substrate radical intermediate ^{5}**16**, formation of the C–O bond occurs concerted with an electron transfer from substrate to iron (TS ^{5}**17H** in Figure 8). The calculated barrier is 8.2 kcal/mol, i.e. 3.7 kcal/mol higher than the corresponding barrier for C–S bond formation (4.5 kcal/mol). Electronically, the two transition states look rather similar with a small amount of spin transferred from the substrate radical to the iron center (see Figure 8). However, hydroxylation requires a rotation of the hydroxo ligand away from its equilibrium position in intermediate ^{5}**16**, where the hydrogen points directly at the substrate carbon radical**.** This leads to an initial increase in energy. Another factor that computationally favors the cyclization reaction is the entropy. A possible explanation of the entropy effect is that hydroxylation anchors the substrate to the iron center at two points (thiolate and hydroxo group) while cyclization leads to a single weak iron-thiol ligation with higher substrate flexibility.

When comparing the two products, the hydroxylated substrate is actually more stable than the observed isopenicillin N product. This is counterintuitive, because the factors disfavoring the hydroxylation transition state should also disfavor the hydroxylation product. However, the transition to a ferrous state leads to changes not directly connected to the transition state, i.e. relaxation of the iron coordination sphere that can favor the new orientation of the hydroxo group. It is also difficult to accurately calculate the relative energy of the two product states. As an example, the entropy calculation may break down for structures with very long and weak metal coordination bonds.

The calculations give the correct energetic ordering of the two transition states, i.e. hydroxylation is more than 100-fold slower than ring formation. The difference in barrier height can be the dominating factor in determining the selectivity of the final reaction step. Still, the energetic separation between the two rebound barriers is relatively small and energy differences in the 3-5 kcal/mol range is at the accuracy limit of the present computational method.

When it comes to the final reaction step, there exist significant similarities between IPNS and the α-keto-acid-dependent halogenases. Halogenases are believed to form a substrate radical through C–H bond activation and the substrate then undergoes halogenation rather than hydroxylation. Recent results from density functional modeling of a biomimetic complex, that catalyze substrate chlorination through a similar route as the halogenases, show that the energetic barriers for the two competing reactions are too similar to explain the observed selectivity (xlv). More detailed calculations, e.g. including the full protein environment, may be required to fully understand the selectivity, both in the halogenases and in isopenicillin N synthase.

SUMMARY AND CONCLUSION

A potential energy surface has been constructed for the enzymatic transformation of ACV to isopenicillin N in IPNS. Three reaction steps show significant barriers (15–18 kcal/mol); activation of the cysteine β-C–H bond by an iron-bound superoxo radical, β-lactam ring formation and activation of the valine β-C–H bond by a ferryl-oxo species. The C-H activation steps are known to be partially rate limiting, and the barriers agree very well with the experimental rate (corresponding to a barrier of 16.8 kcal/mol). The barrier for β-lactam ring formation (18.4 kcal/mol) is relatively high, but this can probably be explained by limitations in the model.

The present study proposes a mechanism for O–O bond cleavage that is different from previous mechanistic proposals. O–O bond cleavage occurs with the help of an iron-ligating water molecule that donates a proton to the distal oxygen and generates the OH–Fe(IV)=O intermediate. The water ligand is regenerated upon closure of the β-lactam ring. The present mechanism for O–O cleavage is almost identical to the reaction in pterin-dependent hydroxylases and very similar to the reaction in α-keto-acid-dependent dioxygenases. Compared to a previous computational study using similar methods, the mechanism for Cys-β-C–H bond activation and β-lactam ring formation is different. The major differences come from a more stable electronic structure of a key intermediate, together with a new, previously untested mechanism for O–O bond cleavage.

The barrier for substrate hydroxylation, a reaction formally competing with thiazolidine ring closure is calculated to be 4 kcal/mol higher than for ring closure. This difference in energy can be a dominating factor in determining the selectivity of the final reaction step.

The calculated potential energy profile can be used for further investigations of reactivity of modified substrates and enzyme mutants. However, such modeling requires a better understanding of substrate interactions with the protein, while still accurately evaluating the reactivity of different substrate molecules. This objective can be achieved by the use of QM:MM models of the IPNS reaction, which is in progress in our laboratory.

Acknowledgements: The use of computational resources at the Fukui Institute for Fundamental Chemistry and at the Research Center of Computer Science (RCCS) at the Institute for Molecular Science (IMS) is acknowledged.

Supporting Information. List of stationary structures along the reaction pathway with energies (in Hartrees), together with structure files (in XYZ format). This material is available free of charge via the Internet at http://pubs.acs.org.

References

i. Schofield, C. J., Baldwin, J. E., Byford, M. F., Clifton, I., Hajdu, J., Hensgens, C., and Roach, P. (1997) Proteins of the penicillin biosynthesis pathway, *Curr. Opin. Struct. Biol. 7*, 857–864.

ii. Baldwin, J. E., and Bradley, M. (1990) Isopenicillin N Synthase: Mechanistic Studies, *Chem. Rev. 90*, 1079–1088.

iii. Schenk, W. A. (2000) Isopenicillin N synthase: An Enzyme at Work, *Angew. Chem. Int. Ed. 39*, 3409–3411.

iv. Roach, P. L., Clifton, I. J., Hensgens, C. M. H., Shibata, N., Schofield, C. J., and Baldwin, J. E. (1997) Structure of isopenicillin N synthase complexed with substrate and the mechanism of penicillin, *Nature 387*, 827–830.

v. Andersson, I., Terwisscha van Scheltinga, A. C., and Valegård, K. (2001) Towards new β-lactam antibiotics, *Cell. Mol. Life Sci. 58*, 1897–1906.

vi. Costas, M., Mehn, M. P., Jensen, M. P., and Que, L. Jr. (2004) Dioxygen Activation at Mononuclear Nonheme Iron Active Sites: Enzymes, Models, and Intermediates, *Chem. Rev. 104*, 939–986.

vii. Koehntop, K. D., Emerson, J. P., and Que, L. Jr. (2005) The 2-His-1-carboxylate facial triad: a versatile platform for dioxygen activation by mononuclear non-heme iron(II) enzymes, *J. Biol. Inor. Chem. 10*, 87–93.

viii. Que, L. Jr., and Ho, R. Y. N. (1996) Dioxygen Activation by Enzymes with Mononuclear Non-Heme Iron Active Sites, *Chem. Rev. 96*, 2607−2624.

ix. Chen, V. J., Orville, A. M., Harpe, M. R., Frolik, C. A., Surerus, K. K., Münck, E., and Lipscomb, J. D. (1989) Spectroscopic Studies of Isopenicillin N Synthase, *J. Biol. Chem. 264*, 21677–21681.

x. Scott, R. A., Wang, S. K., Eidsness, M. K., Kriauciunas, A., Frolik, C. A., and Chen, V. J. (1992) X-ray Absorption Spectroscopic Studies of the High-Spin Iron(II) Active Site of Isopenicillin N Synthase: Evidence for Fe-S Interaction in the Enzyme-Substrate Complex, *Biochemistry 31*, 4596–4601.

xi. Randall, C. R., Zang, Y., True, A. E., Que, L. Jr., Charnock, J. M., Garner, C. D., Fujishima, Y., Schofield, C. J., and Baldwin, J. E. (1993) X-ray Absorption Studies of the Ferrous Active Site of Isopenicillin N Synthase and Related Model Complexes, *Biochemistry 32*, 6664–6673.

xii. Roach, P. L., Clifton, I. J., Fülöp, V., Harlos, K., Barton, G. J., Hajdu, J., Andersson, I., Schofield, C. J., and Baldwin, J. E. (1995) Crystal structure of Isopenicillin N synthase is the first from a new family of enzymes, *Nature 375*, 700–704.

xiii. Burzlaff, N. I., Rutledge, P. J., Clifton, I. J., Hensgens, C. M. H., Pickford, M., Adlington, R. M., Roach, P. L., and Baldwin, J. E. (1999) The reaction cycle of isopenicillin N synthase observed by X-ray diffraction, *Nature 401*, 721–724.

xiv. Long, A. J., Clifton, I. J., Roach, P. L., Baldwin, J. E., Schofield C. J., and Rutledge, P. J. (2003) Structural studies on the reaction of isopenicillin N synthase with the substrate analogue δ-(L-α-aminoadipoyl)-L-cysteinyl-D-α-aminobutyrate, *Biochem. J. 372*, 687–693.

xv. Elkins, J. M., Rutledge, P. J., Burzlaff, N. I., Clifton, I. J., Adlington, R. M., Roach, P. L., and Baldwin, J. E. (2003) Crystallographic studies on the reaction of isopenicillin N synthase with an unsaturated substrate analogue, *Org. Biomol. Chem. 1*, 1455–1460.

xvi. Long, A. J., Clifton, I. J., Roach, P. L., Baldwin, J. E., Rutledge, P. J., Schofield, C. J. (2005) Structural Studies on the Reaction of Isopenicillin N Synthase with the Truncated Substrate Analogues δ-(L-α-aminoadipoyl)-L-cysteinyl-glycine and δ-(L-α-aminoadipoyl)-L-cysteinyl-D-alanine, *Biochemistry 44*, 6619–6628.

xvii. Daruzzaman, A., Clifton, I. J., Adlington, R. M., Baldwin, J. E., and Rutledge, P. J. (2006) Unexpected Oxidation of a Depsipeptide Substrate Analogue in Crystalline Isopenicillin N Synthase, *ChemBioChem, 7*, 351–358.

xviii. Kreisberg-Zakarin, R., Borovok, I., Yanko, M., Frolow, F., Aharonowitz, Y., and Cohen, G. (2000) Structure–function studies of the non-heme iron active site of isopenicillin N synthase: some implications for catalysis, *Biophys. Chem. 86*, 109–118

xix. Borovok, I., Landman, O., Kreisberg-Zakarin, R., Aharonowitz, Y., and Cohen, G. (1996) Ferrous Active Site of Isopenicillin N Synthase: Genetic and Sequence Analysis of the Endogenous Ligands, *Biochemistry 35*, 1981–1987.

xx. Sim, T.-S., and Loke, P. (2000) Molecular studies on isopenicillin N synthase, *Appl. Microbiol. Biotechnol. 54*, 1–8.

xxi. Solomon, E. I., Brunold, T. C., Davis, M. I., Kemsley, J. N., Lee, S.-K., Lehnert, N., Neese, F., Skulan, A. J., Yang, Y. S., and Zhou, J. (2000) Geometric and Electronic Structure/Function Correlations in Non-Heme Iron Enzymes, *Chem. Rev. 100*, 235–349.

xxii. Brown, C. D., Neidig, M. L., Neibergall, M. B., Lipscomb, J. B., and Solomon E. I. (2007) VTVH-MCD and DFT Studies of Thiolate Bonding to $\{FeNO\}^7/\{FeO2\}^8$ Complexes of Isopenicillin N Synthase: Substrate Determination of Oxidase versus Oxygenase Activity in Nonheme Fe Enzymes, *J. Am. Chem. Soc. 129*, 7427–7438.

xxiii. Baldwin, J. E., Adlington, R. M., Moroney, S. E., Field, L. D., and Ting, H.-H. (1984) Stepwise Ring-Closure in Penicillin Biosynthesis - Initial Beta-Lactam Formation, *J. Chem. Soc. Chem. Commun*. 984–986.

xxiv. Wirstam, M., and Siegbahn, P. E. M. (2000) A Mechanistic Study of Isopenicillin N Formation Using Density Functional Theory, *J. Am. Chem. Soc. 122*, 8539–8547.

xxv. Baldwin, J. E., and Abraham E. (1988) The Biosynthesis of Penicillins and Cephalosporins, *Nat. Prod. Rep. 5*, 129–145.

xxvi. Bassan, A., Borowski, T., and Siegbahn, P. E. M. (2004) Quantum chemical studies of dioxygen activation by mononuclear non-heme iron enzymes with the 2-His-1-carboxylate facial triad, *Dalton Trans. 20*, 3153–3162.

xxvii. Bassan, A., Blomberg, M. R. A., Borowski, T., and Siegbahn, P. E. M. (2006) Theoretical studies of enzyme mechanisms involving high-valent iron intermediates, *J. Inorg. Biochem. 100*, 727–743.

xxviii. Kriauciunas, A., Frolik, C. A., Hassell, T. C., Skatrud, P. L., Johnson, M. G., Holbrok, N. I., and Chen, V. J. (1991) The Functional Role of Cysteines in Isopenicillin N Synthase, *J. Biol. Chem. 266*, 11779–11788.

xxix. Frisch, M. J., Trucks, G. W., Schlegel, H. B., Scuseria, G. E., Robb, M. A., Cheeseman, J. R., Montgomery, Jr., J. A., Vreven, T., Kudin, K. N., Burant, J. C., Millam, J. M., Iyengar, S. S., Tomasi, J., Barone, V., Mennucci, B., Cossi, M., Scalmani, G., Rega, N., Petersson, G. A., Nakatsuji, H., Hada, M., Ehara, M., Toyota, K., Fukuda, R., Hasegawa, J., Ishida, M., Nakajima, T., Honda, Y., Kitao, O., Nakai, H., Klene, M., Li, X., Knox, J. E., Hratchian, H. P., Cross, J. B., Bakken, V., Adamo, C., Jaramillo, J., Gomperts, R., Stratmann, R. E., Yazyev, O., Austin, A. J., Cammi, R., Pomelli, C., Ochterski, J. W., Ayala, P. Y., Morokuma, K., Voth, G. A., Salvador, P.,

Dannenberg, J. J., Zakrzewski, V. G., Dapprich, S., Daniels, A. D., Strain, M. C., Farkas, O., Malick, D. K., Rabuck, A. D., Raghavachari, K., Foresman, J. B., Ortiz, J. V., Cui, Q., Baboul, A. G., Clifford, S., Cioslowski, J., Stefanov, B. B., Liu, G., Liashenko, A., Piskorz, P., Komaromi, I., Martin, R. L., Fox, D. J., Keith, T., Al-Laham, M. A., Peng, C. Y., Nanayakkara, A., Challacombe, M., Gill, P. M. W., Johnson, B., Chen, W., Wong, M. W., Gonzalez, C., and Pople, J. A. Gaussian 03, Revision C.02, Gaussian, Inc., Wallingford CT, 2004.

xxx. Becke, A. D. (1993) Density-functional thermochemistry. III. The role of exact exchange, *J. Chem.Phys. 98*, 5648–5652.

xxxi. Siegbahn, P. E. M. (2006) The performance of hybrid DFT for mechanisms involving transition metal complexes in enzymes, *J. Biol. Inorg. Chem. 11*, 695–701.

xxxii. Noodleman, L., and Case, D. A. (1992) Density-Functional Theory of Spin Polarization and Spin Coupling in Iron-Sulfur Clusters, *Adv. Inorg. Chem. 38*, 423–470.

xxxiii. Cances, E., Mennucci, B., and Tomasi, J. (1997) A new integral equation formalism for the polarizable continuum model: Theoretical background and applications to isotropic and anisotropic dielectrics, *J. Chem. Phys. 107*, 3032–3041.

xxxiv. Lundberg, M., and Morokuma, K. (2007) Protein Environment Facilitates O_2 Binding in Non-Heme Iron Enzyme. An Insight from ONIOM Calculations on Isopenicillin N Synthase (IPNS), *J. Phys. Chem. B* 111, 9380-9389.

xxxv. Bassan, A., Blomberg, M. R. A., and Siegbahn, P. E. M. (2003) Mechanism of Dioxygen Cleavage in Tetrahydrobiopterin-Dependent Amino Acid Hydroxylases, *Chem. –Eur. J. 9*, 106–114.

xxxvi. Wirstam, M., Lippard, S. J., and Friesner, R. A. (2003) Reversible Dioxygen Binding to Hemerythrin, *J. Am. Chem. Soc. 125*, 3980–3987.

xxxvii . Blomberg, M. R. A., and Siegbahn, P. E. M. (1997) A comparative study of high-spin manganese and iron complexes, *Theor. Chem. Acc. 97*, 72–80.

xxxviii . Frey, P. A., Hegeman, A. D., and Reed, G. H. (2006) Free Radical Mechanisms in Enzymology, *Chem. Rev. 106*, 3302–3316.

xxxix . Borowski, T., Bassan, A., and Siegbahn, P. E. M. (2004) A Hybrid Density Functional Study of O−O Bond Cleavage and Phenyl Ring Hydroxylation for a Biomimetic Non-Heme Iron Complex, *Inor. Chem. 43*, 3277–3291.

xl. Borowski, T., Bassan, A., and Siegbahn, P. E. M. (2004) Mechanism of Dioxygen Activation in 2-Oxoglutarate-Dependent Enzymes: A Hybrid DFT Study, *Chem.–Eur. J. 10*, 1031–1041.

xli . Borowski, T., Bassan, A., and Siegbahn, P. E. M. (2004) 4-Hydroxyphenylpyruvate Dioxygenase: A Hybrid Density Functional Study of the Catalytic Reaction Mechanism, *Biochemistry 43*, 12331–12342.

xlii . Rohde, J. U., In, J.-H., Lim, M. H., Brennessel, W. W., Bukowski, M. R., Stubna, A., Münck, E., Nam, W., and Que, L. Jr. (2003) Crystallographic and Spectroscopic Characterization of

a Nonheme Fe(IV)=O Complex, *Science 299*, 1037–1039.

xliii . Riggs-Gelasco, P. J., Price, J. C., Guyer, R. B., Brehm, J. H., Barr, E. W., Bollinger, J. M., and Krebs, C. (2004) EXAFS Spectroscopic Evidence for an Fe=O Unit in the Fe(IV) Intermediate Observed during Oxygen Activation by Taurine:α-Ketoglutarate Dioxygenase, *J. Am. Chem. Soc. 126*, 8108–8109.

xliv . Price, J. C., Barr, E. W., Tirupati, B., Bollinger, J. M., and Krebs, C. (2003) The First Direct Characterization of a High-Valent Iron Intermediate in the Reaction of an α-Ketoglutarate-

Dependent Dioxygenase: A High-Spin Fe(IV) Complex in Taurine/α-Ketoglutarate Dioxygenase (TauD) from Escherichia coli, *Biochemistry 42*, 7497–7508.

xlv. Noack, H., and Siegbahn, P. E. M. (2007) Theoretical investigation on the oxidative chlorination performed by a biomimetic non-heme iron catalyst, *J. Biol. Inor. Chem.* Available online. DOI 10.1007/s00775-007-0284-0.

Schemes

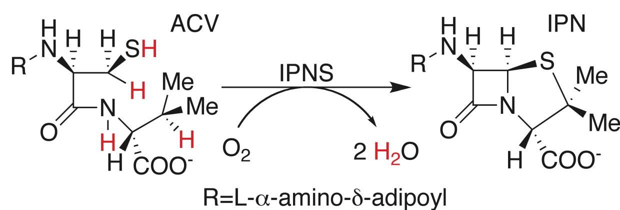

Scheme 1. Enzymatic reaction catalyzed by isopenicillin N synthase (IPNS).

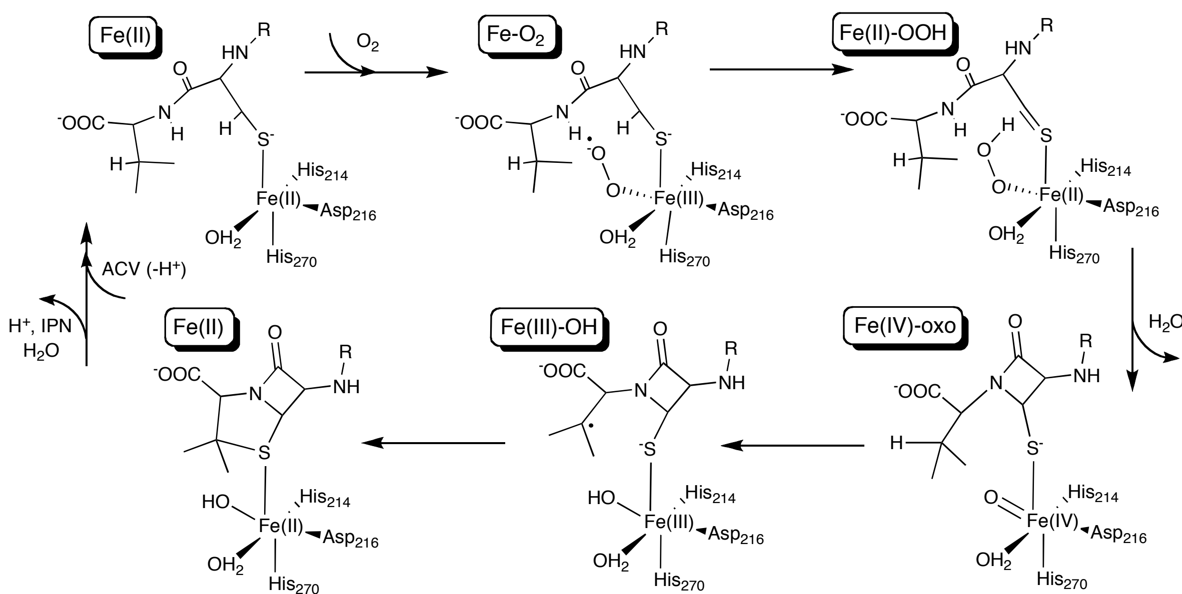

Scheme 2. Proposed scheme for the substrate reaction in isopenicillin N synthase, adapted from reference iv. Binding of oxygen initiates formation of the four-membered β-lactam ring, followed by formation of the five-membered thiazolidine ring.

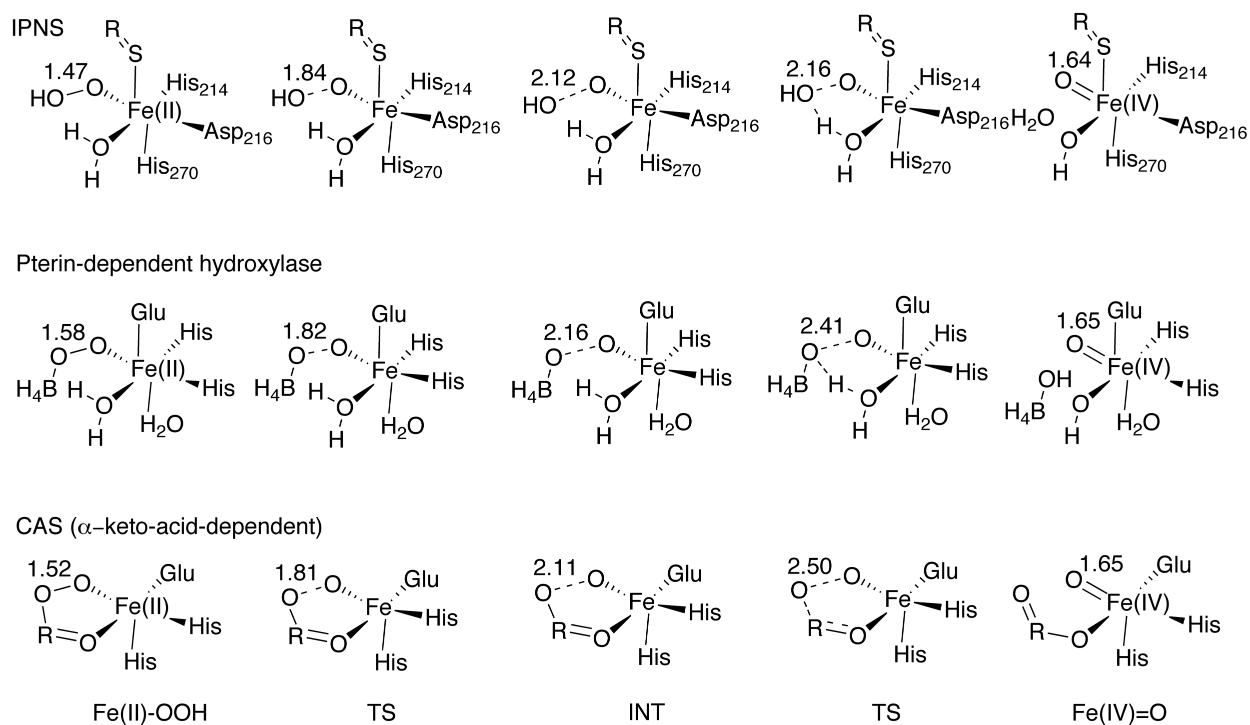

Scheme 3. Similar reaction mechanisms for O–O bond cleavage in three non-heme iron enzymes IPNS (present study), a pterin-dependent hydroxylases (xxxv) and the α-keto-acid-dependent clavaminate synthase (CAS) (xl). Numbers represent O–O bond distances in Å, except for the Fe(IV)=O state where the label shows the iron-oxo distance.

Figure labels

Figure 1. Active site models used in the present study. Atoms whose Cartesian coordinates have been frozen at the X-ray structure are marked with **x**. Model A is used for stationary points **1**–**9**. Model B is used for stationary points **9**–**13** and is derived from model A by removing the substrate carboxylate. Model C is used for stationary points **13–18** and is obtained after removing the water molecule, formed during O–O bond cleavage, from Model B.

Figure 2. Reactant and transition state for Cys-β-C–H activation by a ferric-superoxo (Fe(III)–OO^{-}) species. Labels show selected bond distances (in Å) and Mulliken spin populations.

Figure 3. Calculated potential energy diagram for Cys-β-C–H bond activation on septet, quintet and triplet surfaces. Bold numbers refer to the order of the stationary state, starting from **1** (Fe–O_2 side-on reactant). Numbers in normal font represent relative energies in kcal/mol. The minimum of seam of crossing between septet and quintet surfaces has not been calculated, but the energy should be located close to ^{5}**2**.

Figure 4. Reactant, transition states and intermediate for cleavage of the O–O bond in Fe(II)–OOH leading to formation of an Fe(IV)-oxo species. Labels give selected bond distances (in Å) and important Mulliken spin population.

Figure 5. Calculated potential energy diagram for the enzymatic reaction catalyzed by isopenicillin N synthase. Stationary states are labeled by bold numbers in sequential order. Numbers in normal font are relative energies compared to ^{7}**1** (Fe–O_2 reactant) in kcal/mol.

Intermediate ^{5}**9** is calculated using both Model A and Model B, while intermediate ^{5}**13** is calculated using Models B and C.

Figure 6. Reactant and tentative transition state for closing of the β-lactam ring after formation of an Fe(IV)=O species. Labels give selected bond distances (in Å) and important Mulliken spin populations.

Figure 7. Reactant and transition state for valine β-C–H bond activation. Note that the isopropyl group needs to be rotated before it can be activated by Fe(IV)=O. Labels give selected bond distances (in Å) and important Mulliken spin populations.

Figure 8. Reactant and transition states for formation of the thiazolidine ring (^{5}**17**) and for the competing substrate hydroxylation reaction (^{5}**17H**). Structure labels give selected bond distances (in Å) and important Mulliken spin populations. Relative energies compared to the common intermediate (^{5}**16**) are given in kcal/mol.

Figure 1.

Figure 2.

Figure 3.

Figure 4.

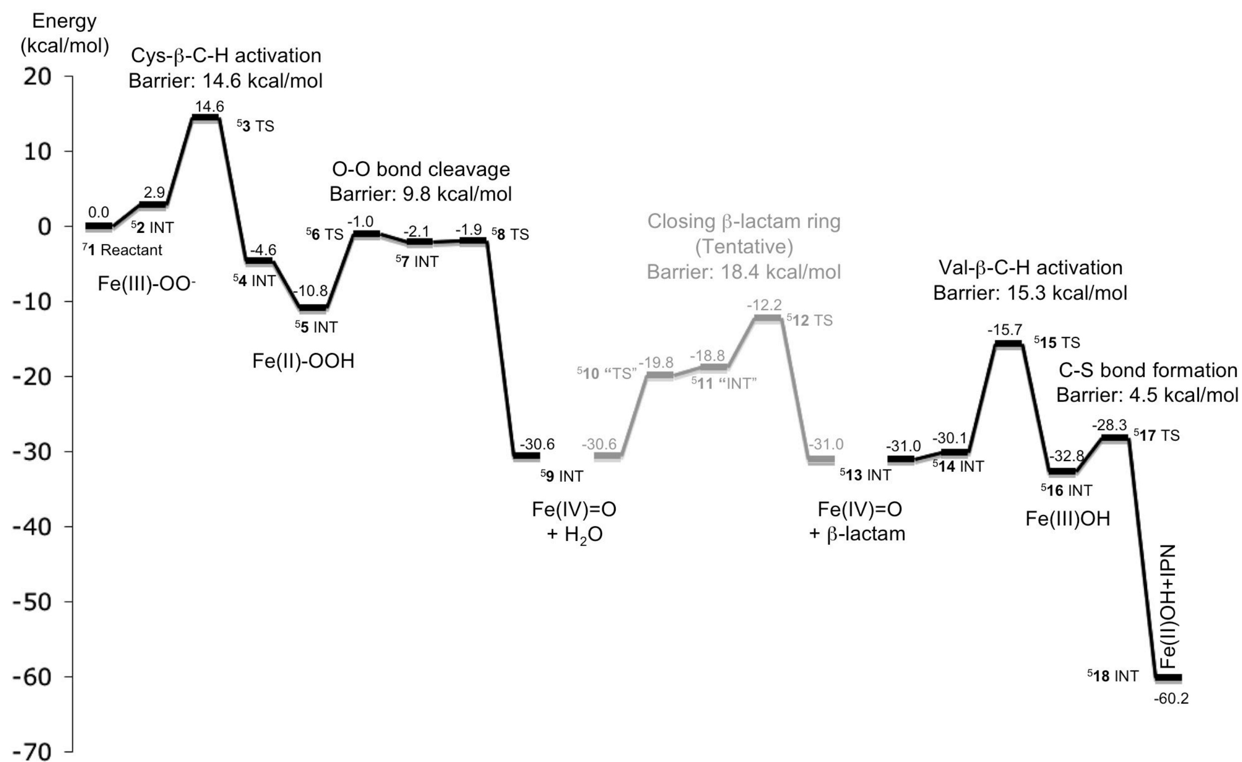

Figure 5.

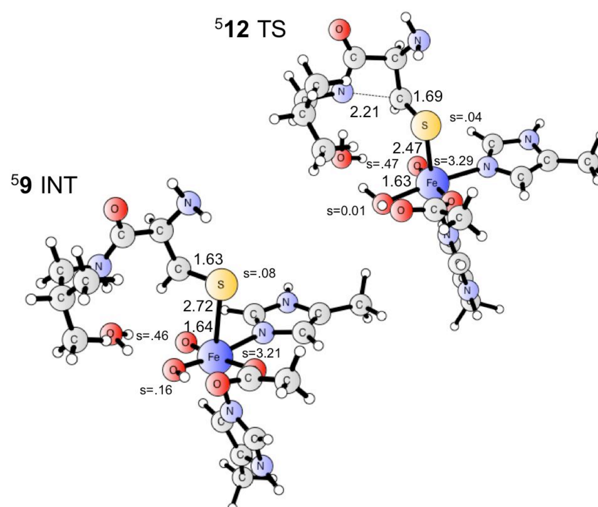

Figure 6.

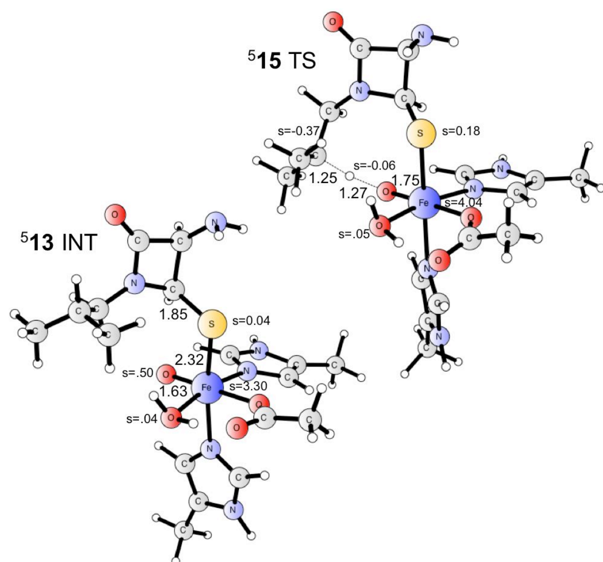

Figure 7.

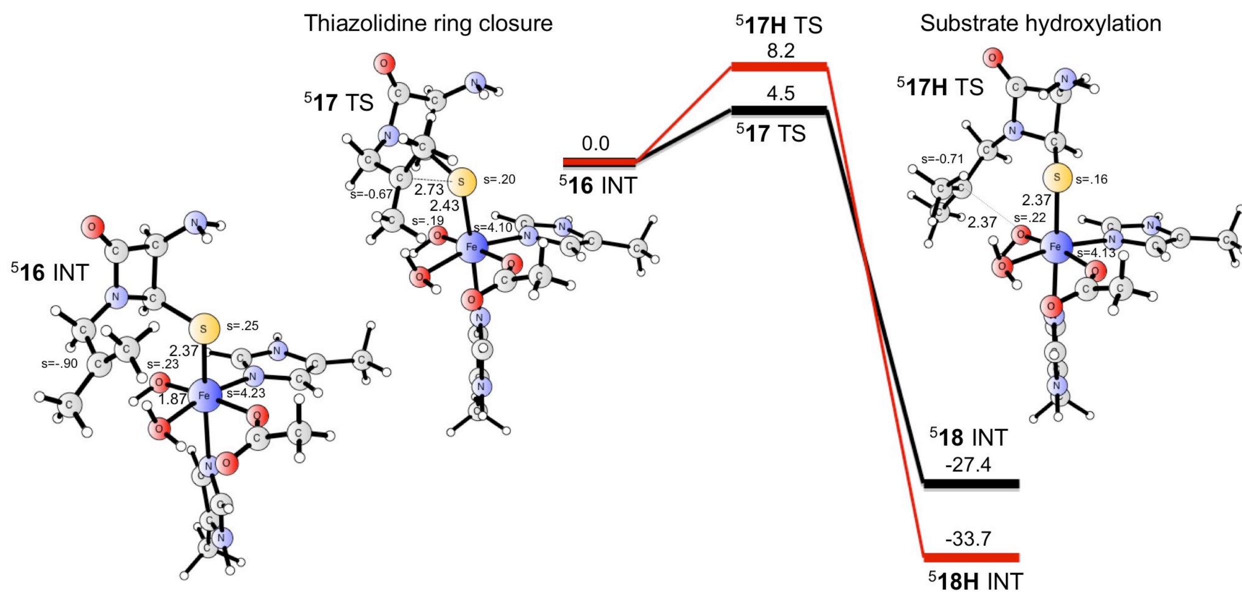

Figure 8.

For Table of Contents use only

Mechanism for Isopenicillin N Synthase from Density-functional Modeling Highlights the Similarities with Other Enzymes in the 2-His-1-carboxylate Family

Marcus Lundberg, Per E. M. Siegbahn, and Keiji Morokuma